Femtosecond Laser Direct Writing of Plasmonic Ag/Pd Alloy Nanostructures Enables Flexible Integration of Robust SERS Substrates

Zhuo-Chen Ma, Yong-Lai Zhang, Bing Han, Xue-Qing Liu, Han-Zhuang Zhang, Qi-Dai Chen, and Hong-Bo Sun*

This paper demonstrates femtosecond laser direct writing mediated flexible integration of plasmonic Ag/Pd alloy nanostructures that can be potentially used as a robust surface-enhanced Raman spectroscopy substrate inside the microfluidic chip. Silver–palladium alloy with controllable composition ratio can be patterned into plasmonic nanostructures due to two-photon absorption induced coreduction of silver/palladium double metal ions. Since the alloy structures can effectively protect the silver from oxidation, thus they can facilitate the stable on-chip detection devices with long lifetime. The as-fabricated silver–palladium alloy substrate with 18% content of palladium maintains a relatively high enhancement factor of about 2.62×10^8 while at the same time demonstrating the best stability against aerobic oxidation, as it is stable for up to 20 d under ambient aerobic conditions, exhibiting a significant improvement compared to those unprotected silver substrates which have a limited lifetime of only 3 or 4 d.

1. Introduction

Surface-enhanced Raman spectroscopy (SERS) that permits fingerprint detection of target analytes at single-molecule level, has been considered as one of the most powerful techniques in analytical chemistry.[1–4] SERS detection is potentially accessible with noble-metal structures or substrates.[5–7] Generally speaking, the rough surface of metals, such as gold or silver, could contribute to a large enhancement of the adsorbed analyte's Raman signals. In recent years, with the rapid progress of microfluidics, the combination of SERS-active substrates with portable microfluidic chips becomes more and more promising for the purpose of developing portable SERS detection devices.[8–12] For example, the integration of SERS substrates within the microfluidic channel enables on-chip detection and in situ monitoring of chemical reactions; the powerful microfluidic systems may, in turn, facilitate high throughput SERS detection, and further promote the efficiency. Thus far, various methods have been proposed to resolve the problem about how to integrate SERS substrates within a microfluidic chip, including metal colloid self-assembly,[9,10] electron beam or physical vapor deposition,[13,14] soft lithography,[15] and the use of natural materials.[16] Although these fabrication techniques have successfully demonstrated the feasibility of making SERS-active microfluidic chips, problems with respect to flexible and localized integration of a SERS substrate inside a microfluidic chip significantly limits their practical application in the development of SERS enabled microfluidic devices.

As a prominent micro-nanofabrication technique, femtosecond laser direct writing (FsLDW)[17–22] possesses unique advantages of arbitrary-shaped patterning, ease of integration, mask-free processing, and suitability for nonplanar substrate. In the past few years, FsLDW technology has revealed its capability in fabrication and integration of highly efficient SERS substrates in microfluidic chips.[23,24] For instance, Xu et al. demonstrated localized and flexible integration of hierarchical silver micro-nanostructures within microfluidic channels by femtosecond laser induced photoreduction of silver ions.[23] Silver SERS substrates could be directly shaped into arbitrary patterns and located at any desired position of the microchannel. In this way, real-time on-chip detection of analytes has been realized using this SERS monitor equipped lab-on-a-chip (LoC) system. Nevertheless, the silver SERS substrates integrated inside the microchannel also suffered from a serious problem. Silver micro-nanostructures could be easily oxidized,[25,26] and thus the stability and lifetime of the SERS enabled LoC system constitutes the main obstacle that hampers its long-term usage. Despite the fact that the stability of silver-based SERS substrates could be improved by coating a stable protective shell, such as titania,[27] silica,[28–30] alumina,[28] or carbon-related materials,[26,31–33] it is inapplicable to employ these methods in dealing with the silver-based SERS substrates

Dr. Z.-C. Ma, Prof. Y.-L. Zhang, Dr. B. Han,
Dr. X.-Q. Liu, Prof. Q.-D. Chen, Prof. H.-B. Sun
State Key Laboratory on Integrated Optoelectronics
College of Electronic Science and Engineering Jilin University
2699 Qianjin Street, Changchun 130012, P. R. China
E-mail: chenqd@jlu.edu.cn
Prof. H.-Z. Zhang, Prof. H.-B. Sun
College of Physics
Jilin University
2699 Qianjin Street, Changchun 130012, P. R. China

DOI: 10.1002/admt.201600270

inside microchannels. Currently, the development of on-chip SERS detection systems with long-term stability is highly desired, but obviously, it remains a technical challenge.

In this paper, we present a coreduction process of silver ion and palladium ion in a single FsLDW step using a relatively stronger reducing agent potassium sodium tartrate for the preparation and integration of silver–palladium (Ag–Pd) alloy nanostructure inside the LoC system. As is well known, silver and palladium are able to form an alloy over the entire composition range,[34,35] and can protect themselves from aerobic oxidation. Moreover, their ability of antioxidation improves with increasing content of palladium. Therefore, this alloy structure can be adopted as a stable and robust substrate for on-ship SERS detection. In our study, Ag–Pd alloy nanostructures with controllable content ratios could be obtained conveniently in one step, without any concern about complex special treatment of the substrates or any strict reaction conditions which were often required in traditional methods of protective shell deposition.[26–33] After a series of experimental comparison, it was found that the alloy substrate containing 18% content of Pd exhibited the best stability with a prolonged lifetime of about 20 d while at the same time maintaining a relatively large enhancement factor of $\approx 2.62 \times 10^8$. The FsLDW technique for silver–palladium alloy nanostructures may thereby hold great promise for the fabrication and integration of SERS-based detection microdevices with high stability.

2. Results and Discussion

In our experiment, by using femtosecond laser induced coreduction approach, the Ag–Pd alloy nanostructures with varying content ratios were successfully fabricated adopting different precursor solutions. **Figure 1** illustrates the schematic of laser direct writing procedure. In the focal region, through two-photon absorption[36,37] process, silver ions and palladium ions were both reduced by the reductant potassium sodium tartrate, thus giving rise to the coprecipitation of these two metals and then the formation of Ag–Pd alloy. The UV–vis absorption spectra of silver precursor solution, Ag–Pd (50/50 mixed) precursor, and palladium precursor solution are shown in Figure S1 (Supporting Information). All these precursors display no obvious absorbance at the excitation wavelength of 800 nm, revealing that a multiphoton absorption process was required for the photoreduction.[38–41]

Using the precursor solutions mixed at different molar ratios, a series of Ag–Pd alloy nanostructures with different compositions were obtained accordingly via femtosecond laser induced photoreduction (**Figure 2**). As the palladium content was increased from 0% to 100% (Figure 2a–e), the surface morphology of the as-fabricated Ag–Pd alloy nanostructures varied significantly, ranging from erect nanoplates (Figure 2f) to assembled metallic grains (Figure 2j), and the surface roughness of these structures is characterized by using atomic force microscopy (AFM), which is shown in Figure S2 (Supporting Information). Figure 2a shows the pure silver nanostructure fabricated by using pure silver precursor solution without palladium ions, which was composed of silver nanoplates with thicknesses in the range of several tens of nanometers, and the

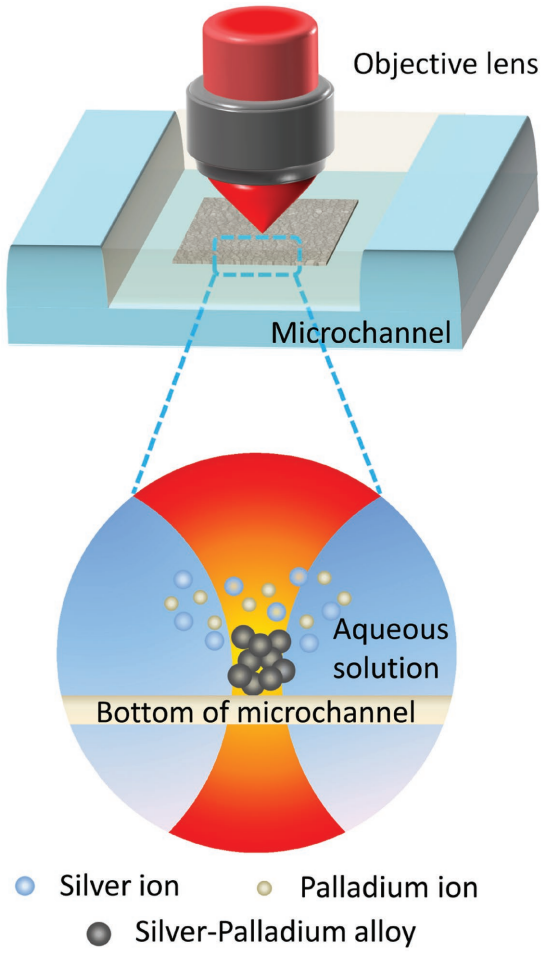

Figure 1. Schematic of the femtosecond laser direct writing enabled integration of Ag–Pd SERS substrates inside the microfluidic channels.

lamella structure of such silver deposit is caused by polarization effect.[42,43] Figure 2e shows the pure palladium nanostructure fabricated by using pure palladium precursor solution, which was made up of palladium grains that were several tens of nanometers in diameter. **Table 1** shows the elemental molar ratios of the Ag–Pd nanostructures, as determined by energy-dispersive X-ray spectrograph (EDS) analysis, and their spectra were demonstrated in Figure S3 (Supporting Information). The elemental ratios of the Ag–Pd nanostructures largely corresponded to the feeding molar ratios, considering the experimental error in elemental ratios determined by EDS, the error brought about during precursor preparation, or the intrinsically different precipitation rates between these two metal ions.

The X-ray diffraction (XRD) spectrum of the sample prepared using the Ag–Pd (90/10 mixed) precursor solution shown in Figure S4 (Supporting Information) further confirmed the bimetallic alloy structure of the coreduction product. Specifically, an intense peak at 38.5° was observed, which was located between the value of pure Ag crystal (111) at 38.1° and pure Pd crystal at 40.0°, confirming the formation of the Ag–Pd alloy.[34,35]

In order to optimize the experimental conditions, the dependence of fabrication resolution on laser power was

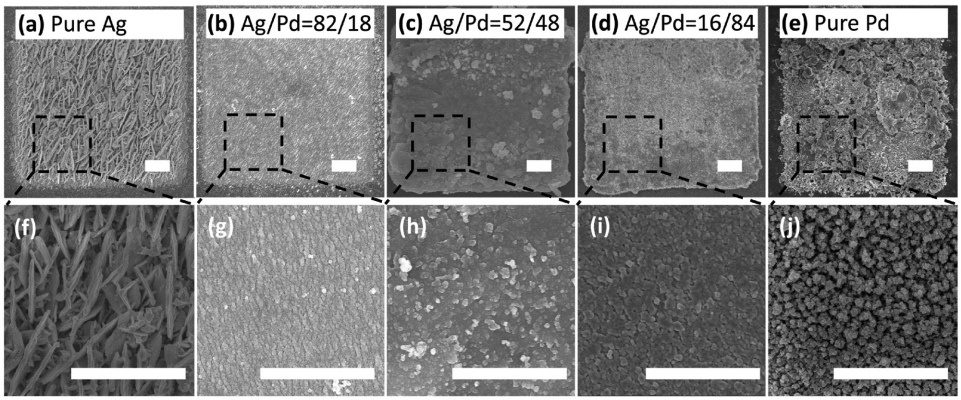

Figure 2. Ag–Pd alloy nanostructures with various compositions could be fabricated through femtosecond laser induced reduction. a–e) The surface morphology of the silver–palladium alloy substrates composed of different metal molar ratios. Scale bar: 1 μm. f–j) The locally magnified images of the structures in (a)–(e), respectively. Scale bar: 1 μm.

evaluated using the Ag–Pd (90/10 mixed) precursor solution. As shown in **Figure 3**a, a series of Ag–Pd alloy nanowires were successfully patterned on glass substrates, the width of which could be readily adjusted by varying the laser power. The thinnest nanowire produced by a laser power of 8 mW was ≈570 nm (Figure 3b), which was relatively larger compared to pure silver nanowire that could approach less than 150 nm,[40] ascribing to the influence of palladium ion photoreduction. In the coreduction procedure of Ag—Pd, due to the presence of palladium ions, obvious bubbles were forced out from the zone of laser induced chemical reaction, therefore leading to a defocusing of the laser beam, which results in a poor resolution.[41] In addition, the threshold laser power for palladium deposition was larger than that of silver (shown in **Table 2**, Supporting Information), which might also contribute to a worse resolution. As shown in Figure 3c,d, arbitrary alloy patterns such as a lion and transformer face could be produced directly on glass substrates, suggesting the flexibility and designability of the femtosecond laser induced reduction of metal ions toward the fabrication and integration of Ag—Pd based SERS substrates.

R6G, which has been extensively used for SERS study previously due to its well-established vibrational features, was adopted as the probe molecule to demonstrate the SERS performance of the alloy substrates. The Raman spectra of 10^{-7} M R6G molecule adsorbed on five freshly prepared metal substrates composed of different ratios of silver and palladium are shown in **Figure 4**. Ascribing to the powerful designability of FsLDW, the SERS substrates could be patterned at any desired position and with desired sizes, indicating the flexible integration capability of this technique. As shown in Figure 4a, SERS substrates with different sizes were successfully integrated in the microchannel bed. After this postintegration process, the probe molecules liquid could be injected into the microchannel via a microsyringe, and then we tested the SERS spectra, which were demonstrated in Figure 4b. In all these experiments, the SERS spectra were acquired under the excitation wavelength of 532 nm. The SERS spectrum of R6G adsorbed on the pure silver substrate exhibited the highest SERS activity in our study. The SERS activity of the Ag—Pd alloy nanostructures decreased notably with increasing palladium contents, and deteriorated rapidly when the content of palladium was increased above 18%. The underlying reason for this phenomenon could be due to the permittivity change of the alloys,[44] which might have a great impact on the SERS enhancement ability. With the purpose of improving the antioxidation ability of the Ag—Pd alloy substrates while maintaining their SERS activity at the same time, we examined only the SERS characteristics of the Ag—Pd alloy nanostructure with a palladium content of 18% in the following experiment.

In order to investigate the stability of the bimetallic alloy nanostructures (with 18% content of Pd), the substrates were subjected to aerobic exposure, and the Raman spectra of R6G

Table 1. The relationship between the feeding molar ratio and EDS atomic ratio.

Feeding molar ratio Ag/Pd	100% Ag	90:10	50:50	10:90	100% Pd
EDS atomic ratio Ag/Pd	100% Ag	82:18	52:48	16:84	100% Pd

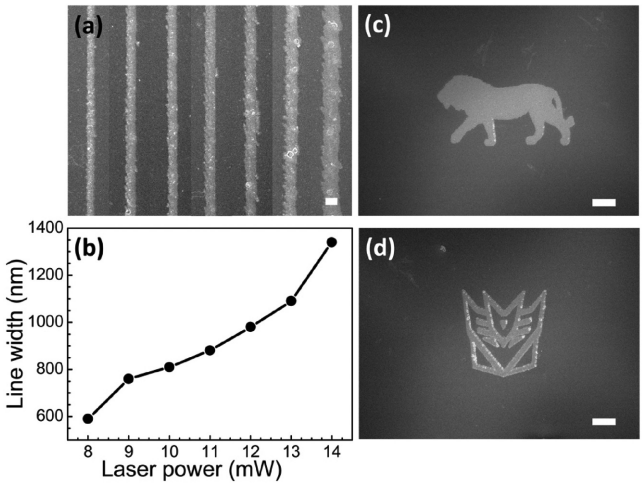

Figure 3. Fabrication of Ag–Pd alloy nanowires and their patterning. a) Ag–Pd alloy nanowires with varying linewidth. Scale bar: 1 μm. b) The dependence of the alloy nanowires width on laser power. c,d) The patterning of Ag–Pd alloy, a lion and a transformer face, respectively. Scale bar: 10 μm.

Table 2. The optical density range for different solutions of Ag–Pd precursors.

Atomic ratio of Ag/Pd	Optical density [W m^{-2}]
100% Ag	(5–14) × 10^{14} W m^{-2}
82:18	(7–18) × 10^{14} W m^{-2}
52:48	(10–34) × 10^{14} W m^{-2}
16:84	(14–42) × 10^{14} W m^{-2}
100% Pd	(16–48) × 10^{14} W m^{-2}

were subsequently collected using the Ag—Pd nanostructure and pure Ag substrate for comparison. Representative Raman spectra measured over 20 d for the Ag–Pd alloy and over 4 d for the Ag substrate are shown in **Figure 5**a,b, respectively. Qualitatively, the fine features and intensities of the signals of the alloy substrates were maintained over a relatively long period (20 d),

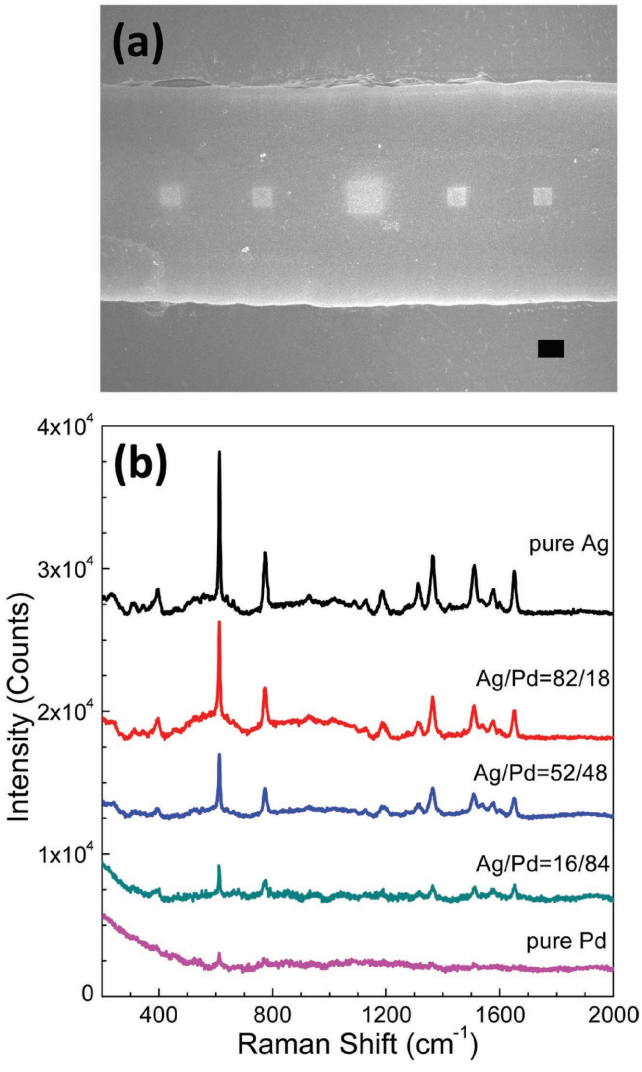

Figure 4. a) SERS substrates integrated in the microfluidic channels. Scale bar: 10 µm. b) SERS spectra of Ag–Pd alloy nanostructures with various metal ratios using 10^{-7} M R6G as the probe molecule.

whereas those of the pure silver substrates displayed an obvious decrease in intensity within just 4 d. Specifically, the intensities of the Raman signals at 1363 and 1509 cm^{-1}, which were assigned to the aromatic and aliphatic C—C stretching modes of R6G, respectively, were monitored and compared. The Raman signal intensities of R6G were calculated by averaging the values of multiple measurements. Variations in the Raman signal intensity versus exposure time are shown in Figure 5c,d for Ag—Pd alloy and pure Ag, respectively. The Raman intensities at these two peaks (1363 and 1509 cm^{-1}) were normalized to those obtained with the freshly prepared samples. For the pure silver substrate (Figure 5d), the Raman intensity of R6G at ≈1363 cm^{-1} dropped to 60% and 27% of its original value after 2 and 4 d of exposure to ambient conditions, respectively; the relative intensity at ≈1509 cm^{-1} dropped to 50% and 25%, as compared to the Raman intensity of the freshly prepared samples. However, under the same exposure condition, the relative intensity of the Ag—Pd alloy (with 18% content of Pd) did not drop to 75% until the 20th day (Figure 5c). This result demonstrated that the alloy substrate exhibited higher stability than silver substrate.

Figure 6 shows the EDS results of Ag/O atomic ratio in different substrates versus exposure time under ambient conditions. After several days of exposure to ambient conditions, the Ag/O atomic ratio of the pure silver substrate on glass whose initial value (the 0 d) was about 3.32, decreased to 2.05 on the fifth day, and 1.37 on the 20th day, while the Ag/O atomic ratio of the Ag—Pd alloy (with 18% content of Pd) only decreased to 2.16 on the 20th day with an initial value of about 2.7. This result revealed that the oxidation rate of the Ag—Pd alloy nanostructure was slowed down compared to the pure silver nanostructure, thus having a positive effect on the stability of SERS substrates.

In order to test the reproducibility of silver–palladium alloy nanostructure (with 18% content of palladium), SERS spectra of R6G molecules (10^{-7} M) from nine different positions on the substrate were collected under identical experiment condition (**Figure 7**a). It can be seen evidently that the Raman spectra taken at randomly selected points are nearly the same, suggesting that the alloy substrate has good reproducibility. Moreover, it should be noted that only slight fluctuations of the peak intensity at 1509 cm^{-1} could be observed with a small relative standard deviation of 5.4%, shown in Figure 7b.

To evaluate the enhancement ability of the alloy nanostructure with 18% content of Pd, the enhancement factor (EF) was calculated according to the following formula[23]

$$\mathrm{EF} = \frac{I_{\mathrm{SERS}} \times N_{\mathrm{bulk}}}{N_{\mathrm{SERS}} \times I_{\mathrm{bulk}}} \quad (1)$$

where I_{SERS} is the intensity of a vibrational mode in the surface-enhanced Raman spectrum, I_{bulk} is the intensity of the same mode in the Raman spectrum, N_{SERS} is the number of molecules adsorbed on the alloy substrate within the laser spot area, and N_{bulk} is the number of molecules excited within the volume of the laser waist in a bulk sample. In our result, the EF value was calculated to be about 2.62 × 10^8, and the detection limit was as low as 10^{-9} M which was shown in Figures S5 and S6 (for details of the calculation, see Supporting Information). As

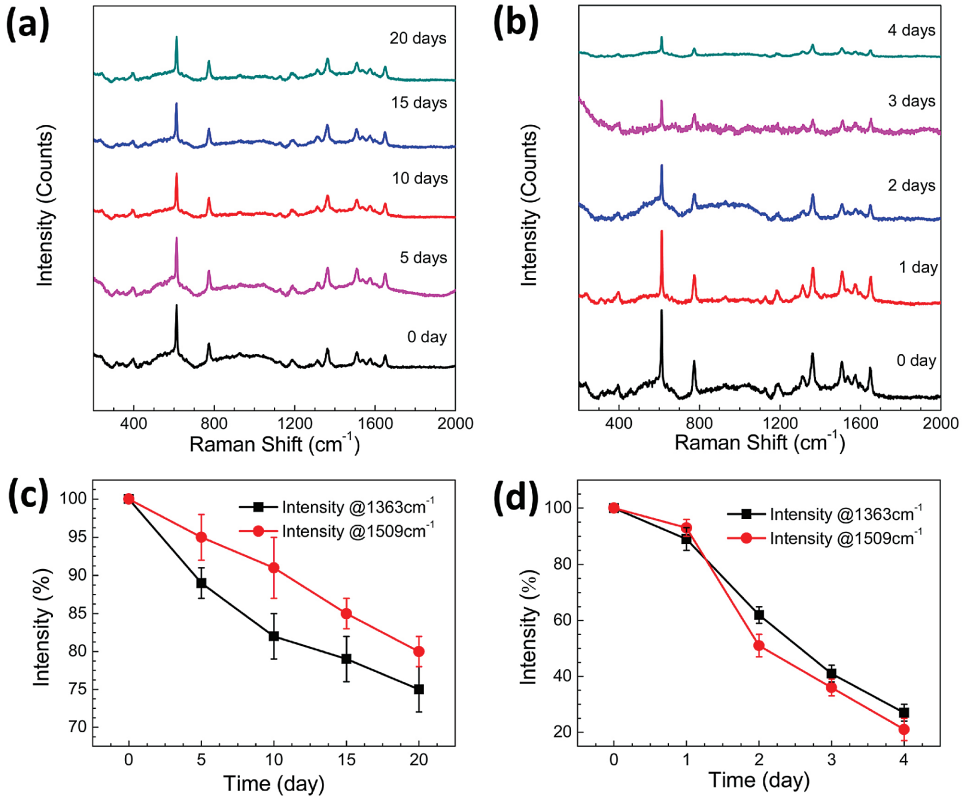

Figure 5. a) SERS spectra of Ag–Pd alloy nanostructures (18% Pd) with increasing exposure time under ambient conditions within 20 d. b) The SERS spectra of pure silver nanostructure with increasing exposure time under ambient conditions within 4 d. c) The variations in SERS intensities of the alloy substrate with 18% palladium at 1363 and 1509 cm^{-1}, respectively. d) The variations in SERS intensities of the silver substrate at 1363 and 1509 cm^{-1}, respectively.

compared to the EF of 4.04×10^8 for the pure silver substrate[23] (shown in Figure 2a), the silver–palladium alloy structure was only slightly less sensitive. Nevertheless, the EF of alloy substrate (2.62×10^8) might be sufficient for SERS-based detection and sensing, which is anticipated to be improved with additional research in our future work.

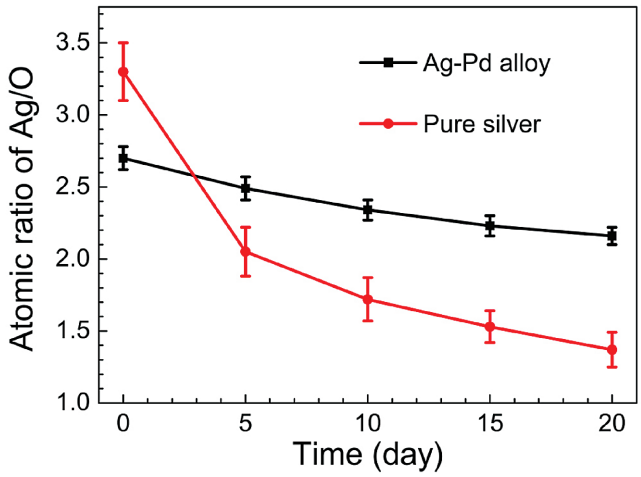

Figure 6. EDS atomic ratios of O/Ag with proceeding exposure period on pure silver and Ag–Pd alloy (18% palladium) substrates within 20 d.

Moreover, to assess the potential of the silver–palladium alloy SERS substrate, a comparison was made regarding the drop in EF over time between the alloy and the pure silver nanostructures (shown in **Figure 8**). The freshly prepared pure silver and silver–palladium alloy substrates exhibited EF of 4.04×10^8 and 2.62×10^8, respectively, in the beginning (on the 0 d), and their EF both decreased with increasing exposure time, but it is evident that the degradation velocity of the pure silver was faster than that of alloy. Notably, on the second day, the EF of alloy had little change, which was still 2.51×10^8, whereas the EF of pure silver dropped significantly and reached 2.26×10^8. Therefore, from the second day on, the silver–palladium alloy began to show a larger EF than the pure silver, and the EF of pure silver deteriorated much more severely than alloy in the following days. Furthermore, after calculation, on the 20th day the EF of alloy still maintained at a relatively high level of $\approx 1.89 \times 10^8$, demonstrating that the as-prepared Ag–Pd alloy nanostructures may hold great potential for application as long-term stable SERS substrates.

3. Conclusion

An on-chip SERS detection device with long-term stability has been fabricated by integrating Ag–Pd alloy nanostructures inside the microfluidic channels. The alloy structures composed

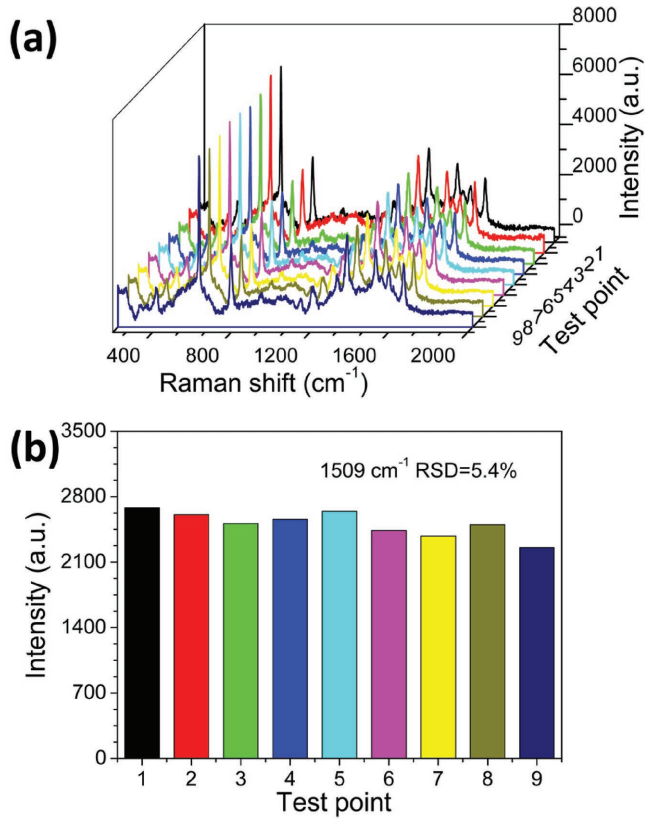

Figure 7. a) SERS spectra of R6G collected on the randomly selected nine points of the Ag–Pd alloy nanostructure. b) Corresponding intensity variation of the peaks at 1509 cm^{-1}.

of varying metal ratios were prepared using a femtosecond laser induced coreduction process. The Ag–Pd alloy with 18% content of Pd showed the best stability against aerobic oxidation, and exhibited sufficient SERS sensitivity, which was stable for up to 20 d under ambient aerobic conditions, revealing a significant improvement in terms of the lifetime. Meanwhile, the alloy substrate exhibited a high EF of about 2.62×10^8, demonstrated superior reproducibility, and could achieve a detection limit of as low as 10^{-9} M. As such, we believe that this strategy will serve as a facile and straightforward route to facilitate the SERS enabled LoC system with long-term usage.

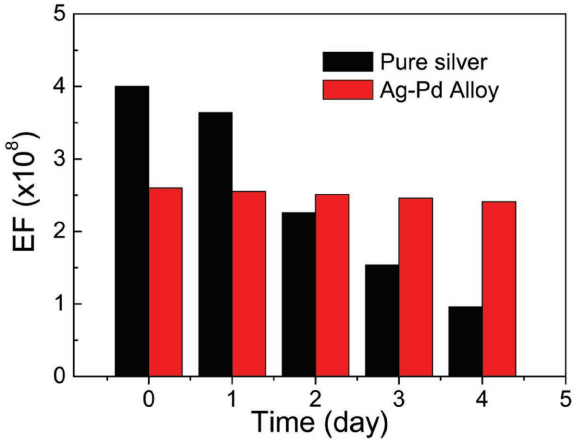

Figure 8. The comparison with respect to the drop in EF over time between the alloy and the pure silver nanostructures. All the enhancement factors are the result of average values after several times of calculation.

4. Experimental Section

Preparation of Precursor Solution: Initially, the precursor solution for the Ag–Pd alloy nanostructures fabrication was prepared by mixing a silver precursor solution and palladium precursor solution at different molar ratios. The silver precursor solution was prepared by dropping a suitable amount of aqueous ammonia into a mixture of silver nitrate (0.1 M) and potassium sodium tartrate (0.1 M) aqueous solution with stirring until a clear solution was formed. The palladium precursor solution was prepared by adding potassium sodium tartrate (0.1 M) to an aqueous solution of 0.1 M $PdCl_2$ and 4 M NH_3. In both cases, potassium sodium tartrate served as a reducing agent for the reduction of silver and palladium ions. Prior to Ag–Pd alloy nanostructure fabrication, the silver and palladium precursor solutions were mixed at molar ratios of 90/10, 50/50, and 10/90, respectively.

Femtosecond Laser Direct Writing: A Ti:sapphire laser system (Spectra-Physics Tsunami) with an output wavelength of 800 nm, a pulse width of 100 fs, and a repetition frequency of 80 MHz was used as a laser source. The laser beam was introduced to an inverted microscope and tightly focused at the interface between the precursor solution and a glass substrate using an oil-immersion objective lens (100×, NA = 1.42). The programmable 3D scanning and fabrication were achieved by the combination of a piezo stage (for sample's vertical movements; PI P-622 ZCD; precision, 1 nm) and a two-galvano-mirror set (for horizontal scanning of laser beam). All the processes of fabrication were controlled by a computer exactly. The patterned alloy nanostructures were rinsed in distilled water for 5 min to remove the residual metal ion solution and then dried under nitrogen atmosphere.

Characterization: The absorption spectra were measured via a Shimadzu UV-2550 spectrophotometer. The surface roughness of the alloys has been detected by using an AFM (Dimension Icon, Bruker) in tapping mode. The surface morphologies of the samples were measured using a JEOL JSM-7500F field emission scanning electron microscope which was equipped with JSM 7001F EDS for element identification. XRD data were recorded on a RigakuD/Max-2550 diffractometer with Cu Kα radiation (λ = 0.15418 nm). Surface enhanced Raman spectra were measured on a JOBIN YVON T64000 equipped with a liquid-nitrogen-cooled argon ion laser at 532 nm (Spectra-Physics Stabilite 2017) as an excitation source. The spectral resolution was about 4 cm^{-1} at the excitation wavelength, the laser power was ≈30 μW on the samples, and the average spot size was 1 μm in diameter.

Supporting Information

Supporting Information is available from the Wiley Online Library or from the author.

Acknowledgements

The authors gratefully acknowledge the financial support from National Natural Science Foundation of China (NSFC) under grants #91423102, #91323301, #61378053, #51335008, and #61590930.

Received: November 25, 2016
Revised: January 25, 2017
Published online: March 15, 2017

[1] Y. Huang, Y. Fang, Z. Zhang, L. Zhu, M. Sun, *Light: Sci. Appl.* **2014**, *3*, e199.
[2] G. Seniutinas, G. Gervinskas, R. Verma, B. D. Gupta, F. Lapierre, P. R. Stoddart, F. Clark, S. L. McArthur, S. Juodkazis, *Opt. Express* **2015**, *23*, 6763.
[3] Y. Yokota, K. Ueno, H. Misawa, *Small* **2011**, *7*, 252.
[4] H. Jung, M. Park, M. Kang, K.-H. Jeong, *Light: Sci. Appl.* **2016**, *5*, e16009.
[5] M. Fleischmann, P. J. Hendra, A. J. McQuillan, *Chem. Phys. Lett.* **1974**, *26*, 163.
[6] M. G. Albrecht, J. A. Creighton, *J. Am. Chem. Soc.* **1977**, *99*, 5215.
[7] D. L. Jeanmaire, R. P. Van Duyne, *J. Electroanal. Chem. Interfacial Electrochem.* **1977**, *84*, 1.
[8] Y. Zhao, Y.-L. Zhang, J.-A. Huang, Z. Zhang, X. Chen, W. Zhang, *J. Mater. Chem. A* **2015**, *3*, 6408.
[9] G. Chen, Y. Wang, H. Wang, M. Cong, L. Chen, Y. Yang, Y. Geng, H. Li, S. Xu, W. Xu, *RSC Adv.* **2014**, *4*, 54434.
[10] L. X. Quang, C. Lim, G. H. Seong, J. Choo, K. J. Do, S.-K. Yoo, *Lab Chip* **2008**, *8*, 2214.
[11] J. Leem, H. W. Kang, S. H. Ko, H. J. Sung, *Nanoscale* **2014**, *6*, 2895.
[12] J. Parisi, Q. Dong, Y. Lei, *RSC Adv.* **2015**, *5*, 14081.
[13] R. M. Connatser, L. A. Riddle, M. J. Sepaniak, *J. Sep. Sci.* **2004**, *27*, 1545.
[14] Y.-J. Oh, K.-H. Jeong, *Adv. Mater.* **2012**, *24*, 2234.
[15] B.-B. Xu, Z.-C. Ma, H. Wang, X.-Q. Liu, Y.-L. Zhang, X.-L. Zhang, R. Zhang, H.-B. Jiang, H.-B. Sun, *Electrophoresis* **2011**, *32*, 3378.
[16] J.-A. Huang, Y.-L. Zhang, Y. Zhao, X.-L. Zhang, M.-L. Sun, W. Zhang, *Nanoscale* **2016**, *8*, 11487.
[17] D. Wu, J. Xu, L.-G. Niu, S.-Z. Wu, K. Midorikawa, K. Sugioka, *Light: Sci. Appl.* **2015**, *4*, e228.
[18] W. Xiong, Y. S. Zhou, W. J. Hou, L. J. Jiang, Y. Gao, L. S. Fan, L. Jiang, J. F. Silvain, Y. F. Lu, *Sci. Rep.* **2014**, *4*, 4892.
[19] J.-J. Park, P. Prabhakaran, K. K. Jang, Y. Lee, J. Lee, K. Lee, J. Hur, J.-M. Kim, N. Cho, Y. Son, D.-Y. Yang, K.-S. Lee, *Nano Lett.* **2010**, *10*, 2310.
[20] Z. Lao, Y. Hu, C. Zhang, L. Yang, J. Li, J. Chu, D. Wu, *ACS Nano* **2015**, *9*, 12060.
[21] T. W. Lim, Y. Son, Y. J. Jeong, D.-Y. Yang, H.-J. Kong, K.-S. Lee, D.-P. Kim, *Lab Chip* **2011**, *11*, 100.
[22] W. Xiong, Y. S. Zhou, X. N. He, Y. Gao, M. Mahjouri-Samani, L. Jiang, T. Baldacchini, Y. F. Lu, *Light: Sci. Appl.* **2012**, *1*, e6.
[23] B.-B. Xu, Z.-C. Ma, L. Wang, R. Zhang, L.-G. Niu, Z. Yang, Y.-L. Zhang, W.-H. Zheng, B. Zhao, Y. Xu, Q.-D. Chen, H. Xia, H.-B. Sun, *Lab Chip* **2011**, *11*, 3347.
[24] M. Focsan, A. M. Craciun, S. Astilean, P. L. Baldeck, *Opt. Mater. Express* **2016**, *6*, 1587.
[25] M. Erol, Y. Han, S. K. Stanley, C. M. Stafford, H. Du, S. Sukhishvili, *J. Am. Chem. Soc.* **2009**, *131*, 7480.
[26] F. Liu, Z. Cao, C. Tang, L. Chen, Z. Wang, *ACS Nano* **2010**, *4*, 2643.
[27] T. Hirakawa, P. V. Kamat, *J. Am. Chem. Soc.* **2005**, *127*, 3928.
[28] J. F. Li, Y. F. Huang, Y. Ding, Z. L. Yang, S. B. Li, X. S. Zhou, F. R. Fan, W. Zhang, Z. Y. Zhou, Y. WuDe, B. Ren, Z. L. Wang, Z. Q. Tian, *Nature* **2010**, *464*, 392.
[29] W. Wang, Z. Li, B. Gu, Z. Zhang, H. Xu, *ACS Nano* **2009**, *3*, 3493.
[30] S. P. Mulvaney, M. D. Musick, C. D. Keating, M. J. Natan, *Langmuir* **2003**, *19*, 4784.
[31] X. Li, J. Li, X. Zhou, Y. Ma, Z. Zheng, X. Duan, Y. Qu, *Carbon* **2014**, *66*, 713.
[32] Y. Liu, Y. Hu, J. Zhang, *J. Phys. Chem. C* **2014**, *118*, 8993.
[33] Y.-K. Kim, S. W. Han, D.-H. Min, *ACS Appl. Mater. Interfaces* **2012**, *4*, 6545.
[34] L. Chen, Y. Liu, *J. Colloid Interface Sci.* **2011**, *364*, 100.
[35] F. Lu, D. Sun, J. Huang, M. Du, F. Yang, H. Chen, Y. Hong, Q. Li, *ACS Sustainable Chem. Eng.* **2014**, *2*, 1212.
[36] E. Kabouraki, A. N. Giakoumaki, P. Danilevicius, D. Gray, M. Vamvakaki, M. Farsari, *Nano Lett.* **2013**, *13*, 3831.
[37] K. Obata, A. El-Tamer, L. Koch, U. Hinze, B.N. Chichkov, *Light: Sci. Appl.* **2013**, *2*, e116.
[38] Y.-L. Sun, W.-F. Dong, L.-G. Niu, T. Jiang, D.-X. Liu, L. Zhang, Y.-S. Wang, Q.-D. Chen, D.-P. Kim, H.-B. Sun, *Light: Sci. Appl.* **2014**, *3*, e129.
[39] T. Baldacchini, A.-C. Pons, J. Pons, C. N. LaFratta, J. T. Fourkas, Y. Sun, M. J. Naughton, *Opt. Express* **2005**, *13*, 1275.
[40] Y.-Y. Cao, N. Takeyasu, T. Tanaka, X.-M. Duan, S. Kawata, *Small* **2009**, *5*, 1144.
[41] L. D. Zarzar, B. S. Swartzentruber, J. C. Harper, D. R. Dunphy, C. J. Brinker, J. Aizenberg, B. Kaehr, *J. Am. Chem. Soc.* **2012**, *134*, 4007.
[42] B.-B. Xu, L. Wang, Z.-C. Ma, R. Zhang, Q.-D. Chen, C. Lv, B. Han, X.-Z. Xiao, X.-L. Zhang, Y.-L. Zhang, K. Ueno, H. Misawa, H.-B. Sun, *ACS Nano* **2014**, *8*, 6682.
[43] S. Rekštytė, T. Jonavičius, D. Gailevičius, M. Malinauskas, V. Mizeikis, E. G. Gamaly, S. Juodkazis, *Adv. Opt. Mater.* **2016**, *4*, 1209.
[44] Y. Hashimoto, G. Seniutinas, A. Balcytis, S. Juodkazis, Y. Nishijima, *Sci. Rep.* **2016**, *6*, 25010.